Journal of Materials Chemistry B

Accepted Manuscript

ROYAL SOCIETY OF CHEMISTRY

www.rsc.org/materialsB

Journal Name

RSCPublishing

ARTICLE

Multifunctional Biodegradable Mesoporous Microspheres of Eu^{3+}-doped Amorphous Calcium Phosphate: Microwave-Assisted Preparation, pH-Sensitive Drug Release and Bioimaging

Cite this: DOI: 10.1039/x0xx00000x

Received ooth January 2012,
Accepted ooth January 2012

DOI: 10.1039/x0xx00000x

www.rsc.org/

Feng Chen,[a,b] Peng Huang,[b] Chao Qi,[a] Bing-Qiang Lu,[a] Xin-Yu Zhao,[a] Chao Li,[b] Jin Wu,[a] Da-Xiang Cui*[b] and Ying-Jie Zhu*[a]

The biodegradable inorganic mesoporous materials hold a promise for various biomedical applications such as drug/gene delivery, bioimaging, photodynamic/photothermal and ultrasound therapy. Herein, multifunctional mesoporous microspheres of europium-doped amorphous calcium phosphate (Eu^{3+}-doped ACP) have been prepared using a natural biomolecule adenosine triphosphate (ATP) by the rapid microwave-assisted solvothermal method. This method has advantages such as surfactant-free, rapidness and energy-saving. The ATP molecule plays key roles as a phosphate source and a structure mediator. Furthermore, the Eu^{3+}-doped ACP mesoporous microspheres exhibit advantages such as high specific surface areas (from 253 to 315 m^2 g^{-1}), high biocompatibility, pH-responsive drug release, and *in vitro/in vivo* fluorescent imaging properties. The mechanism of pH-responsive drug release can be explained by the degradation of ACP mesoporous microspheres in lower pH solution. The docetaxel-loaded Eu^{3+}-doped ACP mesoporous microspheres show a good anticancer performance *in vitro*. The as-prepared Eu^{3+}-doped ACP mesoporous microspheres are promising for applications in drug delivery, tissue engineering, and bioimaging, etc.

1 Introduction

Inorganic biomaterials with good biocompatibility show unique properties of high thermal/chemical stability and resistance to corrosion under physiological conditions. A variety of inorganic biomaterials such as rare earth oxides, noble metals, iron oxides and silica have been investigated for applications in various biomedical fields. For example, rare earth based materials exhibit excellent optical properties which can be used in bioimaging;[1-3] nanostructured noble metals such as gold have been investigated for bioimaging and thermal therapy;[4-7] carbon based materials such as carbon nanotubes, graphene and carbon dots have also been investigated for the biomedical applications.[8-12] Furthermore, the research on mesoporous inorganic materials with well-defined size, morphology and porosity has become a hot topic. Mesoporous silica and its composite materials with ordered or disordered network of mesoporous channels have potential applications in drug delivery, magnetic resonance imaging and fluorescence imaging.[13-17] However, mesoporous inorganic materials such as rare earth materials, noble metals, carbon based materials exhibit relatively poor biodegradation behavior which limits their *in vivo* applications in biomedical fields.

Calcium phosphates (CaPs) including hydroxyapatite can be widely found in nature, especially in the hard tissues of the vertebrate.[18-21] The synthetic CaP based nanostructured materials have been deemed to be bio-friendly and not recognized as foreign materials in the body, due to their similar chemical properties to the inorganic constituent of bone.[22] The synthetic CaP materials exhibit excellent biocompatibility and biodegradability. In the past decades, a variety of CaP based nanostructured materials with different morphologies including nanoparticles, nanorods, nanotubes, plate-like nanocrystals, and three-dimensional structures have been prepared.[23] In addition, the multifunctional CaP materials have also been developed through incorporating functional elements, materials and molecules, and they exhibit various properties such as magnetism, fluorescence, antibacterial and so on.[24-30] Although many achievements have been made, there are still many deficiencies for the CaP based materials which do not meet the high requirements of applications. For example, the synthesis of CaP nanostructured materials with well-defined structure, size, morphology and functions is a long-term challenge. To explore new synthetic methods which can solve these problems is still a big challenge for nanostructured CaP biomaterials.

Inorganic phosphorus sources such as phosphate ions are usually adopted for the synthesis of CaP materials. However, in the precursor solution with supersaturated calcium ions and phosphate ions, rapid nucleation and disordered growth of calcium phosphates may occur, and it is difficult to control the morphology and size of the products. Recently, our research group reported a new strategy for the synthesis of CaP nanostructured biomaterials using the biocompatible phosphorus-containing biomolecules in aqueous solution. For example, fructose 1,6-bisphosphate trisodium salt (FBP), creatine phosphate and pyridoxal-5'-phosphate were used as the organic phosphorus source for the preparation of CaP nanostructured materials.[31–33] Compared with the inorganic phosphorus sources, the use of phosphorus-containing biomolecules as the organic phosphorus sources has many advantages. For instance, phosphorus-containing biomolecules are essentially non-toxic with high biocompatibility and exist in vivo; the phosphorus source is present in biomolecules and no free phosphate ions exist in the reaction solution, thus preventing fast nucleation and disordered growth of calcium phosphates; the hydrolysis of phosphorus-containing biomolecules to form phosphate ions usually require certain conditions such as heating in aqueous solution, and the hydrolysis conditions can be adjusted to control the structure, size, and morphology of the products; the hydrolysis process of phosphorus-containing biomolecules to form phosphate ions is in a progressive manner, therefore avoiding the fast nucleation and disordered growth of calcium phosphates; and the biomolecules can regulate the crystal growth of CaP.[33]

Herein, multifunctional biodegradable mesoporous microspheres of europium-doped amorphous calcium phosphate (ACP) have been prepared by the rapid microwave-assisted solvothermal method. The as-prepared europium-doped ACP mesoporous microspheres exhibit advantages including high specific surface area, pH-responsive drug release, fluorescent imaging properties, and so on, thus, they are promising for the applications in multifunctional drug delivery systems and tissue engineering scaffolds with bio-imaging-guidance, etc.

2 Experimental

2.1 Preparation of ACP mesoporous microspheres

In a typical experiment, 0.147 g $CaCl_2 \cdot 2H_2O$ was dissolved in mixed solvent of 10 mL deionized water and 20 mL ethylene glycol. Then, 1 mL aqueous solution of 1 M NaOH and 10 mL aqueous solution containing 0.330 g adenosine triphosphate disodium salt (ATP) were added dropwise to the above solution under magnetic stirring at room temperature, respectively. The resulting solution was loaded into a 60 mL autoclave, sealed and microwave-heated in a microwave oven (MDS-6, Sineo, China) to 120 °C and maintained at this temperature for 10 min, and cooled down to room temperature naturally. Then the product was separated, and washed with deionized water and ethanol several times. For the preparation of Eu^{3+}-doped ACP mesoporous microspheres, an aqueous solution containing europium nitrate was added into the calcium chloride solution before mixing with ATP solution. The doping concentration of Eu^{3+} was 2.5, 5 and 10 mol% relative to Ca^{2+}, respectively.

2.2 Characterization

X-ray powder diffraction (XRD) patterns were recorded using a X-ray diffractometer (Rigaku D/max 2550V, Cu K_α radiation, λ = 1.54178 Å). Fourier transform infrared (FTIR) spectra were taken on a FTIR spectrometer (FTIR-7600, Lambda Scientific, Australia). Scanning electron microscopy (SEM) micrographs were performed with a field-emission scanning electron microscope (FEI, Magellan-400, USA). Transmission electron microscopy (TEM) micrographs and energy dispersive spectroscopy (EDS) were taken with a JEOL JEM 2100 field-emission transmission electron microscope. The thermogravimetric (TG) analysis was carried out with a STA-409/PC simultaneous thermal analyzer (Netzsch, Germany) at a heating rate of 10 °C min^{-1} in flowing air. The Brunauer-Emmett-Teller (BET) specific surface area and pore size distribution were measured with a surface area and pore size analyzer (V-sorb 2800P, Gold APP Instruments). The photoluminescent (PL) measurements were carried out on a spectrofluorometer (Fluorolog−3, Jobin Yvon) at room temperature.

2.3 Drug loading and in vitro drug release

The typical drug loading and *in vitro* drug release experiments were performed as follows: the dried powder (100 mg) of the as-prepared Eu^{3+}-doped ACP mesoporous microspheres was dispersed in 5 mL ethanol solution with a docetaxel (Dtxl) concentration of 20 mg mL^{-1}. The suspension was treated under ultrasonic for 1 h, and then was shaken in a sealed vessel at 37 °C for 24 h, followed by centrifugation and dried to obtain the Eu^{3+}-doped ACP mesoporous microsphere drug delivery system. For the drug release assay, 5 mg Eu^{3+}-doped ACP mesoporous microsphere drug delivery system was immersed into 8 mL of phosphate buffered saline (PBS, pH = 7.4 and 4.5) at 37 °C with a constant shaking (140 rpm). The shaking device was a desk-type constant-temperature oscillator (THI-92A, China). The release medium (0.4 mL) was withdrawn for analysis by UV-vis absorption spectroscopy at a wavelength of 230 nm at given time intervals and replaced with the same volume of fresh PBS solution.

2.4 pH-sensitive degradability

pH-sensitive degradability of the as-prepared sample was studied. The typical experiment was performed as follows: 5 mg of dried powder of as-prepared sample was dispersed into 5 mL deionized water with different pH values (pH = 2, 4.5, 7.4 and 9), respectively. Thereafter, the solutions were shaken in sealed vessels at 37 °C at a constant shaking rate (140 rpm). The medium (0.4 mL) was withdrwn for analysis by inductively coupled plasma optical emission spectrometry (ICP-OES, JY2000-2, Horiba) at given time intervals and replaced with the same volume of fresh deionized water.

2.5 In vitro cell viability

The human gastric carcinoma (MGC−803) cells, which were cultured in a RPMI−1640 medium supplemented with 10% fetal bovine serum (FBS) and 1% penicillin–streptomycin at 37 °C for 48 h, were used for cell viability tests. Then, the cells were seeded in 96 well flat−bottom microassay plates at a concentration of 1×10^4 cells mL^{-1} and cultured for 24 h. The sterilized Eu^{3+}-doped ACP mesoporous microspheres were added into wells at the concentrations from 10 to 100 μg mL^{-1}, and were co-cultured with cells for 48 h. The sample free tissue culture plate was used as a control. The cell viability was quantified by the 3-(4,5-dimethylthiazol-2-yl)-2,5-diphenyltetrazolium bromide (MTT) assay, and the data are representative as the mean value of three parallel experiments. All reagents used in cell viability experiments were purchased from Sigma-Aldrich.

2.6 In vitro and in vivo fluorescence imaging

For *in vitro* fluorescence imaging study, 5 mol % Eu^{3+}-doped ACP mesoporous microspheres were dispersed in PBS with a concentration of 0, 1, 5 and 10 mg mL^{-1}, respectively. Then, the *in vitro* fluorescence images of the solutions were obtained. For *in vivo* fluorescence imaging study, the male nude mice weighing 20~22 g were purchased from Shanghai SLAC Laboratory Animal Co. Ltd. Animals were maintained in the animal care facility and housed eight per cage at room temperature (22 ± 2 ºC). All animal procedures were in accord with institutional animal use and care regulations. The nude mice were randomized into two groups with three animals per group, including the control group and subcutaneous injection group. For the subcutaneous injection experiments, the mice were anesthetized with 100 μL of 10 % chloral hydrate, and placed on an animal plate heated to 37 °C. Then, 100 μL of PBS containing 5 mol % Eu^{3+}-doped ACP mesoporous microspheres (with a concentration of 10 mg mL^{-1}) was subcutaneously injected into the left flank area of mice. *In vitro* and *in vivo* fluorescence images were recorded on a Cambridge Research & Instrumentation (CRi) *in vivo* imaging system (CRi, MA, USA) using 490 nm longpass as the emission filter.

3 Results and discussion

3.1. Synthesis and SEM, TEM and XRD characterization of as-prepared ACP mesoporous microspheres

The morphology of the samples synthesized using an organic phosphate source of ATP biomolecule by the microwave-assisted solvothermal method at 120 ºC for 10 min was characterized by scanning electron microscopy (SEM) (Fig. S1 in Supplementary Information). From these SEM micrographs, one can see that all the samples consist of mesoporous microspheres which are formed by self-assembly with small nanoparticles. The mesoporous microspheres have sizes of several hundred nanometers and small pores with diameters ranging from 10 to 20 nm.

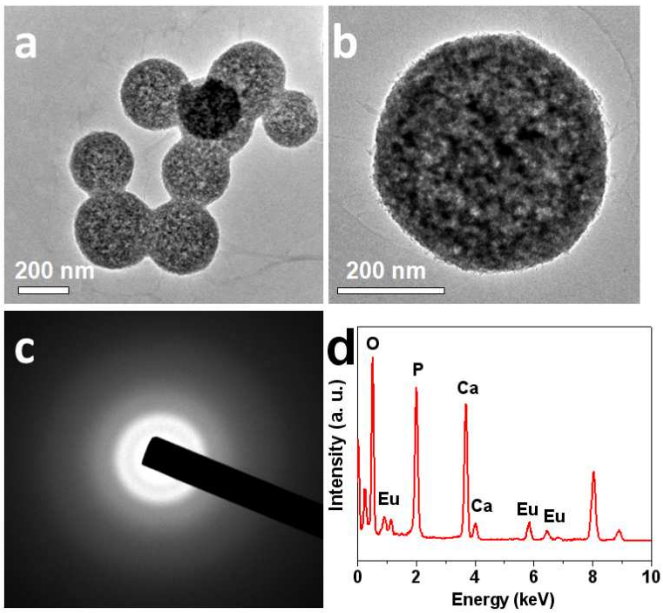

Fig. 1. TEM micrographs (a,b), SAED pattern (c) and EDS spectrum (d) of 5 mol % Eu^{3+}-doped ACP mesoporous microspheres prepared using ATP as an organic phosphate source by the microwave-assisted solvothermal method.

The morphology of the as-prepared 5 mol% Eu^{3+}-doped ACP mesoporous microspheres was also investigated with transmission electron microscopy (TEM). One can see that the sample consists of mesoporous microspheres with diameters ranging from 200 to 300 nm (Fig. 1a,b). The selected area electron diffraction (SAED) pattern of the as-prepared mesoporous microspheres shows a diffraction pattern of amorphous structure (Fig. 1c). The chemical composition of Eu^{3+}-doped ACP mesoporous microspheres were characterized by energy dispersive spectroscopy (EDS) (Fig. 1d), which clearly indicates the presence of europium in the product.

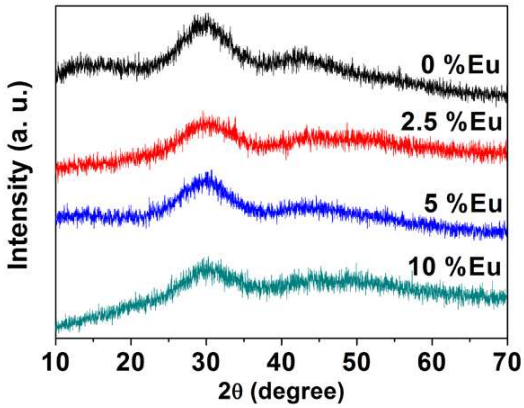

Fig. 2. The XRD patterns of the undoped ACP mesoporous microspheres and Eu^{3+}-doped ACP mesoporous microspheres with different Eu^{3+} doping concentrations (mol %) relative to Ca^{2+} prepared using ATP as an organic phosphate source by the microwave-assisted solvothermal method.

The X-ray powder diffraction (XRD) patterns (Fig. 2) of undoped ACP and Eu^{3+}-doped ACP mesoporous microspheres exhibit no discernable peaks of crystalline calcium phosphate but a characteristic hump of the amorphous phase at around $2\theta = 30^{o}$, indicating that all the samples consist of the amorphous CaP phase.[34] This result agrees with the SAED result (Fig. 1c). ACP is an important kind of CaP materials and is present in the natural bone. Thus, ACP is promising for applications in many biomedical fields. Compared with hydroxyapatite, ACP is bioactive with better biodegradability, and can promote osteoblast adhesion and osteoconductivity.[35,36]

3.2. Formation of as-prepared ACP mesoporous microspheres

ATP is a most important energy carrier of the cell in the biological system, and it plays an important role in various life activities. ATP can transport chemical energy within cells for metabolism through the hydrolysis under the catalysis of ATPase. The phosphate ions formed by hydrolysis are used by the body for physiological metabolism. Furthermore, ATP molecules also play a key role in the synthesis of inorganic CaP in bone tissue through supplying energy and phosphate ion source. Based on the above, one can see that there are natural connections between ATP molecules and CaP in the body. Due to these favorable properties, ATP molecules have been chosen and used to design and synthesize ACP materials with a mesoporous structure in this work. The process of preparation and possible formation mechanism of ACP mesoporous microspheres are depictured in Fig. 3.

The possible formation mechanism of the ACP mesoporous microspheres may be explained by the use of ATP which acts as a phosphate source and a structural mediator. Firstly, ATP molecules can hydrolyze to form adenosine diphosphate (ADP), adenosine monophosphate (AMP) and adenosine under microwave heating in aqueous solution, and simultaneously release phosphate ions. Secondly, small primary ACP nuclei form by the reaction between calcium ions and phosphate ions. Finally, the small ACP nuclei grow and self-assemble to form mesoporous microspheres. During the formation process, adenosine based biomolecules may adsorb on ACP mesoporous microspheres, and these biomolecules play an important role in the stabilization of the ACP phase by acting as the stabilizer to inhibit the phase transformation from ACP to hydroxyapatite in aqueous solution. The adsorption of adenosine based biomolecules on the ACP mesoporous microspheres is supported by the Fourier transform infrared (FTIR) spectra (Fig. S2 in Supplementary Information). The strong peak at 1649 cm^{-1} is attributed to the C=C stretching vibration which originates from adenosine. The intense absorption peaks located at around 1122 and 563 cm^{-1} are ascribed to the characteristic peaks of CaP. The peaks at 1400, 924 and 733 cm^{-1} originate from adenosine.

3.3 Hydrodynamic size distribution, zeta potential, BET specific surface area and BJH pore size distribution of Eu^{3+}-doped ACP mesoporous microspheres

The hydrodynamic size distributions of Eu^{3+}-doped ACP mesoporous microspheres with different Eu^{3+} doping concentrations prepared using ATP as an organic phosphate source by the microwave-assisted solvothermal method were measured by DLS in deionized water, and the results are shown in Fig. S3 in Supplementary Information. The average hydrodynamic size of the undoped ACP mesoporous microspheres is 585 nm. When Eu^{3+} ions are doped into ACP mesoporous microspheres, the average hydrodynamic size decreases. The average hydrodynamic size of Eu^{3+}-doped ACP mesoporous microspheres decreases from 506.5 to 239.7 nm with increasing Eu^{3+} doping concentration from 2.5 to 10 mol% (Fig. 4a). The experimental results indicate that the size of ACP mesoporous microspheres can be substantially decreased by increasing the doping concentration of Eu^{3+} ions. The size decrease by Eu^{3+} doping can be explained by different chemical properties of Eu^{3+} ions from Ca^{2+} ions in terms of oxidation state, ionic radius and other properties, which may have effects on the formation process of ACP mesoporous microspheres. The zeta potentials of Eu^{3+}-doped ACP mesoporous microspheres were also measured (Fig. 4b). The zeta potential of the undoped ACP mesoporous microspheres is –25.77 mV. When the Eu^{3+} doping concentration increases from 2.5 to 10 mol%, the value of zeta potential changes from –21.92 to –17.39 mV.

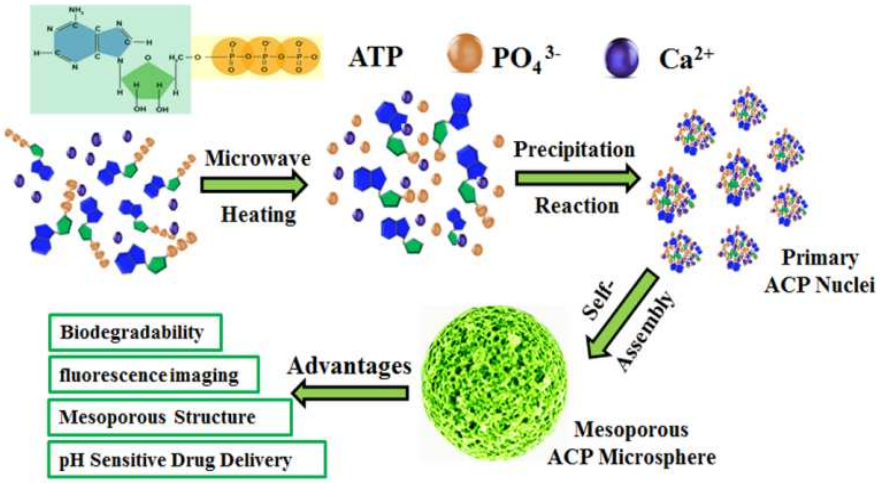

Fig. 3. The proposed formation process of the as-prepared ACP mesoporous microspheres.

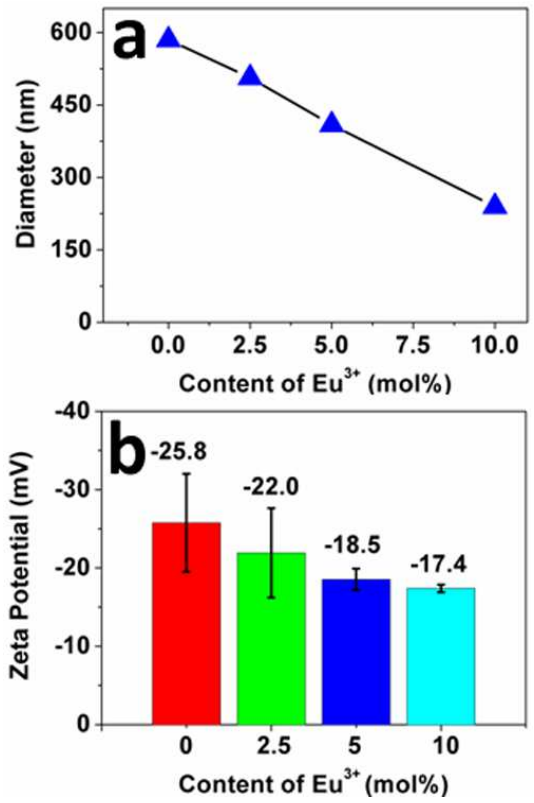

Fig. 4. The average hydrodynamic sizes (a) and zeta potential (b) of Eu^{3+}-doped ACP mesoporous microspheres with doping concentrations of 0, 2.5, 5 and 10 mol %.

Fig. S4 in Supplementary Information shows the nitrogen adsorption-desorption isotherms and the corresponding Barrett-Joyner-Halenda (BJH) pore size distributions of the as-prepared Eu^{3+}-doped ACP mesoporous microspheres with Eu^{3+} doping concentrations from 0 to 10 mol%. According to the International Union of Pure and Applied Chemistry, all the nitrogen adsorption-desorption isotherms can be classified as a type-IV isotherm loop.[37] The BET specific surface area, BJH desorption cumulative pore volume and average pore size of undoped ACP mesoporous microspheres is 209 $m^2 g^{-1}$, 1.12 $cm^3 g^{-1}$ and 17.8 nm, respectively. The specific surface area of undoped ACP mesoporous microspheres is relatively large compared with other CaP materials. Furthermore, when the Eu^{3+} ions are doped into the ACP mesoporous microspheres, the value of BET specific surface area is further increased to 253, 268 and 315 $m^2 g^{-1}$ corresponding to the Eu^{3+} doping concentrations of 2.5, 5 and 10 mol %, respectively. These specific surface areas of Eu^{3+}-doped ACP mesoporous microspheres are very high for CaP materials.

The average pore size of Eu^{3+}-doped ACP mesoporous microspheres decreases with increasing Eu^{3+} doping concentration, in the following decreasing order 17.8, 15.6, 12.6 and 10.1 nm corresponding to the Eu^{3+} doping concentration of 0, 2.5, 5 and 10 mol %, respectively (Fig. 5), and this result is different with the change trend of the BET specific surface area. The BET specific surface areas and pore volumes of many CaP based materials are relatively low (<100 $m^2 g^{-1}$, <0.3 $cm^3 g^{-1}$).[28, 38-40] The BET specific surface area of the CaP material prepared using a non-ionic surfactant of F127 or P123 was reported to be about 263 $m^2 g^{-1}$.[41] Compared with other CaP materials, the as-prepared Eu^{3+}-doped ACP mesoporous microspheres show ultrahigh BET specific surface areas (253 to 315 $m^2 g^{-1}$) and high pore volumes (1.11 to 1.39 $cm^3 g^{-1}$).

The high BET specific surface areas of the as-prepared Eu^{3+}-doped ACP mesoporous microspheres can be explained by the formation of the mesoporous structure. Compared with other synthesis methods, the use of ATP biomolecules provides a powerful manner to control the chemical composition, structure, size and morphology of the product. On the other hand, the increase in BET specific surface area after Eu^{3+} doping can also be explained by different chemical properties of Eu^{3+} ions from Ca^{2+} ions such as ionic radius. Compared with the use of surfactants in the synthesis of inorganic mesoporous materials, the use of ATP biomolecules help improve the biocompatibility of the product. The ultrahigh BET specific surface area, high pore volume and mesoporous structure of the as-prepared Eu^{3+}-doped ACP mesoporous microspheres are favorable for the applications in drug delivery and other biomedical fields.

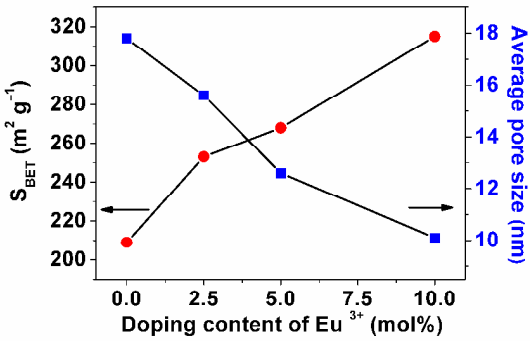

Fig. 5. The changes of BET specific surface area and average BJH pore size of undoped and Eu^{3+}-doped ACP mesoporous microspheres with different Eu^{3+} doping concentrations.

3.4 Photoluminescence properties of Eu^{3+}-doped ACP mesoporous microspheres

Photoluminescence (PL) excitation and emission spectra of the as-prepared Eu^{3+}-doped ACP mesoporous microspheres measured at room temperature are shown in Fig. 6. From the excitation spectra (Fig. 6a), one can see that the most intense excitation peak is located at 393 nm. There are three peaks appeared at about 592, 612 and 696 nm at an excitation of 393 nm in the PL emission spectra (Fig. 6b). These intense emission peaks correspond to the $^5D_0 \rightarrow {}^7F_1$, $^5D_0 \rightarrow {}^7F_2$ and $^5D_0 \rightarrow {}^7F_4$ transitions within Eu^{3+} ions, respectively. These results indicate that the PL intensity changes considerably by varying Eu^{3+} doping concentrations from 0 to 10 mol%. The highest PL emission intensity is observed in the sample with 5 mol% Eu^{3+} doping.

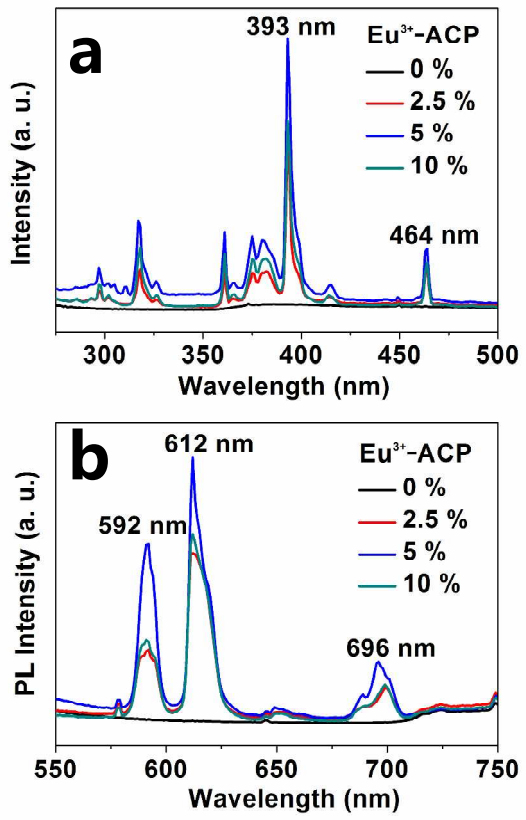

Fig. 6. Room−temperature excitation spectra (a) and PL emission spectra (b) of the as-prepared Eu^{3+}-doped ACP mesoporous microspheres prepared usingATP as an organic phosphate source by the microwave-assisted solvothermal method. The Eu^{3+} doping concentrations are 0, 2.5, 5 and 10 mol % relative to Ca^{2+} in the samples.

3.5 The drug loading and release performance of Eu^{3+}-doped ACP mesoporous microspheres

The drug loading and release performance of the as-prepared Eu^{3+}-doped ACP mesoporous microsphere drug delivery system were investigated using a typical antitumor drug of Dtxl. TG analysis of the samples before and after Dtxl loading was employed to estimate the drug loading capacity. As shown by the TG curves in Fig. 7a, the Dtxl loading capacity of the Eu^{3+}-doped ACP mesoporous microspheres is about 172 mg g^{-1}. The Dtxl drug release behavior of the Eu^{3+}-doped ACP mesoporous microsphere drug delivery system was studied in phosphate buffered saline (PBS) with different pH values (7.4 and 4.5) at 37 °C. As shown in Fig. 7b, Dtxl can rapidly release (about 40 %) from the Eu^{3+}-doped ACP mesoporous microspheres in about 5 h in both PBS solutions with pH values of 7.4 and 4.5. However, the Eu^{3+}-doped ACP mesoporous microsphere drug delivery system exhibits a stable and slow cumulative release level of Dtxl at a higher pH value (pH 7.4) after the initial drug release stage. In contrast, the cumulative release percentage of Dtxl in PBS with a lower pH value of 4.5 reaches a higher level of about 68%, 88% and 92% at the release time of 24, 40 and 60 h, respectively. Then, the cumulative drug release percentage is stable at about 92 % from 60 to 108 h. The higher cumulative Dtxl release percentage at a lower pH value may be attributed to increased dissolution of the ACP mesoporous microspheres in an acidic environment. In the aqueous solution with a lower pH value (pH 4.5), the Eu^{3+}-doped ACP mesoporous microsphere drug delivery system can gradually dissolve, and then Dtxl in mesoporous microspheres releases into the solution.

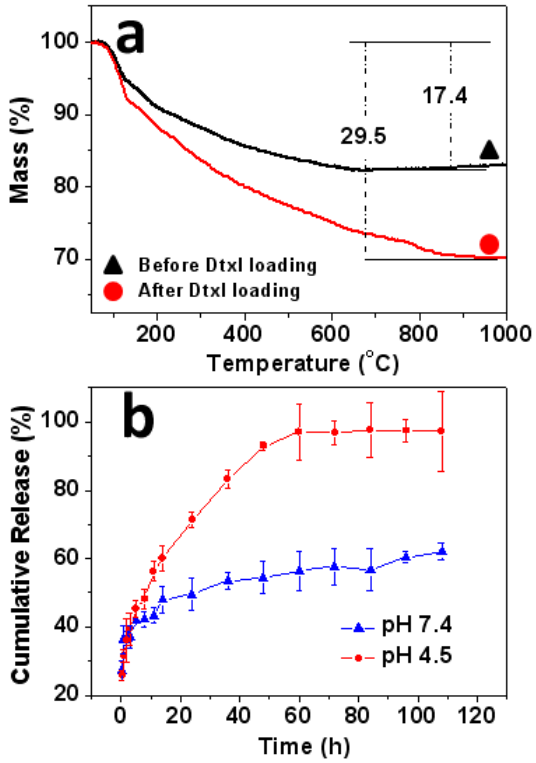

Fig. 7. (a) TG curves of 5 mol% Eu^{3+}-doped ACP mesoporous microspheres before and after Dtxl drug loading; (b) the cumulative Dtxl drug release percentage of 5 mol% Eu^{3+}-doped ACP mesoporous microsphere drug delivery system in PBS with different pH values of 7.4 and 4.5.

The biodegradation behaviors of Eu^{3+}-doped ACP mesoporous microspheres were studied by analyzing the dissolution of the sample in aqueous solutions with different pH values of 2, 4.5, 7.4 and 9. As shown in Fig. 8, the Eu^{3+}-doped ACP mesoporous microspheres exhibit different degrees of dissolution measured by the quantitative analysis of Ca^{2+} and PO_4^{3-} ions released from Eu^{3+}-doped ACP mesoporous microspheres in aqueous solutions with different pH values. The cumulative dissolution percentage of Ca^{2+} ions is 97.9, 67.6, 12.5, and 6.9 % at a time period of 1 h in aqueous solutions with the pH values of 2, 4.5, 7.4 and 9, respectively. Thereafter, the Ca^{2+} ions are completely dissolved at 6 h in an aqueous solution with a pH 2. In the aqueous solution with a pH value of 4.5, the cumulative dissolution percentage of Ca^{2+} ions is 72.4, 89.3 and 96.4 % at 6, 24 and 48 h, respectively.

There is a steady-state increase region for Ca^{2+} dissolution from 0.5 to 48 h at pH 4.5. In contrast, it is difficult for Ca^{2+} dissolution at high pH values of 7.4 and 9. The cumulative dissolution percentage curves of PO_4^{3-} ions show the similar trend to that of Ca^{2+} dissolution. The experimental results indicate that the as-prepared Eu^{3+}-doped ACP mesoporous microspheres have a favourable pH-controlled dissolution property which enables a pH-sensitive drug release.

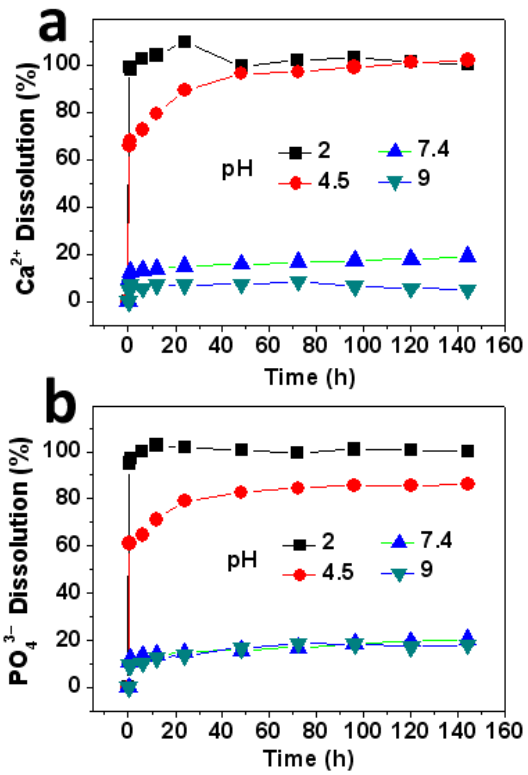

Fig. 8. Ca^{2+} dissolution percentages (a) and PO_4^{3-} dissolution percentages (b) of 5 mol% Eu^{3+}-doped ACP mesoporous microspheres in aqueous solutions with different pH values of 2, 4.5, 7.4 and 9.

3.6 Cytotoxicity tests of Eu^{3+}-doped ACP mesoporous microspheres

The cytotoxicity tests of Eu^{3+}-doped ACP mesoporous microspheres without and with Dtxl loading were performed using MGC−803 cells. The results of 3-(4,5-dimethylthiazol-2-yl)-2,5-diphenyltetrazolium bromide (MTT) assay show no appreciable toxicity when the cells were co-cultured with Eu^{3+}-doped ACP mesoporous microspheres without Dtxl loading at concentrations in the range of 0.1−100 μg mL^{-1} (Fig. 9). The high biocompatibility of Eu^{3+}-doped ACP mesoporous microspheres without Dtxl loading may be explained by similar chemical nature of as-prepared ACP mesoporous microspheres to the hard tissues. Furthermore, in the presence of Dtxl-loaded Eu^{3+}-doped ACP mesoporous microspheres, the cell viability gradually decreased with increasing concentration. The cell viability is only 22.6 and 13.4 % at the concentrations of the sample of 1 and 10 μg mL^{-1}, respectively. These results indicate that the Dtxl-loaded Eu^{3+}-doped ACP mesoporous microspheres are promising for the applications in the biomedical fields.

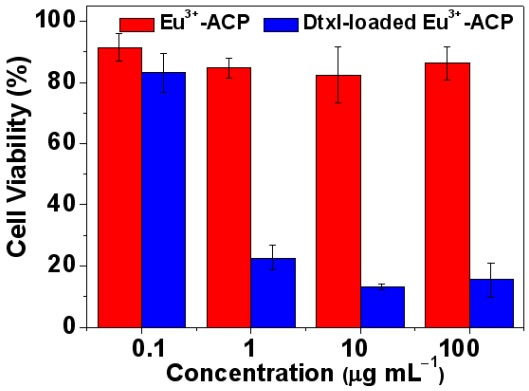

Fig. 9. Cell viability tests of 5 mol% Eu^{3+}-doped ACP mesoporous microspheres without and with Dtxl loading.

3.7 In vitro and in vivo fluorescence imaging

The multifunctional systems hold a promise for the applications in future clinical treatment to enhance therapeutic efficacy.[42,43] It is highly desirable to develop novel multifunctional systems that can achieve high-performance diagnosis and simultaneous medical treatment. Due to their chemical properties, the ACP mesoporous microspheres are favorable for the design of the novel biodegradable multifunctional systems. Therefore, the applicability of the as-prepared Eu^{3+}-doped ACP mesoporous microspheres for fluorescence imaging was investigated *in vitro and in vivo* (Fig. 10). The as-prepared Eu^{3+}-doped ACP mesoporous microspheres exhibit a strong fluorescence, as shown in Fig. 10b. The intensity of the fluorescence increases with increasing concentration of Eu^{3+}-doped ACP mesoporous microspheres. As shown in Fig. 10c, the average fluorescence signal intensity increases from 1612 to 2957 ($\times 10^6$, p/s/cm^2/sr) with increasing concentration of Eu^{3+}-doped ACP mesoporous microspheres from 1 to 2 mg mL^{-1}. Then, the fluorescence emission spectrum was also obtained using the Eu^{3+}-doped ACP mesoporous microsphere solution with a concentration of 2 mg mL^{-1} by the *in vivo* imaging system. The highest peak in the fluorescence emission spectrum appears around the wavelength of 610 nm (Fig. 10d), which is similar to the result of PL spectrum (Fig. 6b).

To demonstrate the feasibility of the as-prepared Eu^{3+}-doped ACP mesoporous microspheres for *in vivo* fluorescence imaging, Eu^{3+}-doped ACP mesoporous microspheres were subcutaneously injected into the mice (100 μL with a concentration of 10 mg mL^{-1} per animal). As shown in Fig. 10e–g, the corresponding subcutaneous injection site of the mice in the Eu^{3+}-doped ACP mesoporous microspheres administrated group displayed a clearly distinguished fluorescence signal. These results indicate that the as-prepared

Eu^{3+}-doped ACP mesoporous microspheres are promising for the application in fluorescence imaging *in vivo*.

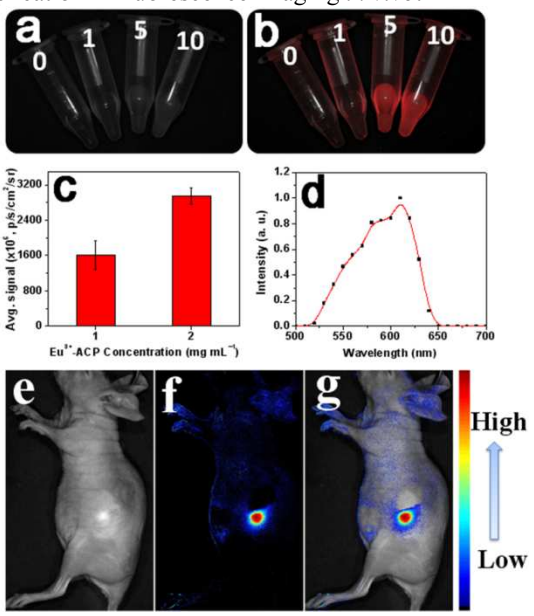

Fig. 10. The *in vitro* visible light image (a) and fluorescence imaging (b) of PBS solutions containing 5 mol% Eu^{3+}-doped ACP mesoporous microspheres with concentrations of 0, 1, 5 and 10 mg mL^{-1}; the average fluorescence signal intensities (c) and the fluorescence emission spectrum (d) obtained using the solution of 5 mol% Eu^{3+}-doped CaP mesoporous microspheres; and *in vivo* visible light image (e), fluorescence image (f), and overlaid image (g) of the nude mice after subcutaneous injection with 5 mol% Eu^{3+}-doped ACP mesoporous microspheres (100 uL, 10 mg mL^{-1}).

4 Conclusions

A natural biomolecule of ATP has been chosen and used to synthesize the Eu^{3+}-doped ACP mesoporous microspheres by the microwave-assisted solvothermal method. The as-prepared undoped and Eu^{3+}-doped ACP mesoporous microspheres show an amorphous phase, and are formed by self-assembly with nanoparticles. In this method, ATP plays a critical role in the formation of ACP mesoporous microspheres, by acting as a phosphate source and structural/chemical phase mediator. Compared with the surfactants used in the preparation of inorganic mesoporous materials, ATP as a natural biomolecule has excellent biocompatibility and is nontoxic. When 10% mol Eu^{3+} ions are doped into ACP mesoporous microspheres, the average hydrodynamic size, pore size and BET specific surface area of the ACP mesoporous microspheres change from 585 to 239.7 nm, 17.8 to 10.1 nm, and 209 to 315 m^2 g^{-1}, corresponding to the Eu^{3+} doping concentrations from 0 to 10 mol %, respectively. The anticancer drug of docetaxel has been used for drug loading and release experiments, the loading capacity of the Eu^{3+}-doped ACP mesoporous microspheres is 172 mg g^{-1}. Furthermore, the pH-sensitive drug release property of Eu^{3+}-doped ACP mesoporous microsphere drug delivery system has been observed in aqueous solutions with different pH values of 4.5 and 7.4. The *in vitro* degradation investigation indicates that the higher cumulative docetaxel release percentage at a lower pH value may be attributed to the increased dissolution of the Eu^{3+}-doped ACP mesoporous microspheres in a lower pH environment. The cell viability assays show no appreciable toxicity when the cells were co-cultured with the Eu^{3+}-doped ACP mesoporous microspheres. The cell viability is only 22.6 and 13.4 % in the presence of the docetaxel-loaded Eu^{3+}-doped ACP mesoporous microspheres at the concentrations of 1 and 10 μg mL^{-1}, respectively. Furthermore, the Eu^{3+}-doped ACP mesoporous microspheres administrated mice group displays a clearly distinguished fluorescence signal *in vitro* and *in vivo*. It is significant to develop Eu^{3+}-doped ACP mesoporous microspheres which are promising for applications in various biomedical fields such as multifunctional drug delivery systems and tissue engineering scaffolds with bioimaging guidance.

Acknowledgements

The financial support from the National Basic Research Program of China (973 Program, No. 2012CB933600, No. 2010CB933901), the National Natural Science Foundation of China (51472259, 51172260, 51102258), and Fund for Youth Scholar of State Key Laboratory of High Performance Ceramics and Superfine Microstructure is gratefully acknowledged.

Notes and references

[a] State Key Laboratory of High Performance Ceramics and Superfine Microstructure, Shanghai Institute of Ceramics, Chinese Academy of Sciences, Shanghai 200050, P. R. China. E-mail: y.j.zhu@mail.sic.ac.cn
[b] Department of Bio-Nano Science and Engineering, Research Institute of Micro/Nano Science and Technology, Shanghai Jiao Tong University, Shanghai 200240, P. R. China. E-mail: dxcui@sjtu.edu.cn

1. Y. Yang, Y. Sun, T. Y. Cao, J. J. Peng, Y. Liu, Y. Q. Wu, W. Feng, Y. J. Zhang, F. Y. Li, *Biomaterials,* 2013, **34**,774.
2. Y. Sun, J. J. Peng, W. Feng, F. Y. Li, *Theranostics*, 2013, **3**, 346.
3. A. Xia, Y. Gao, J. Zhou, C. Y. Li, T. S. Yang, D. M. Wu, L. M. Wu, F. Y. Li, *Biomaterials*, 2011, **32**, 7200.
4. P. Huang, J. Lin, S. J. Wang, Z. J. Zhou, Z. M. Li, Z. Wang, C. L. Zhang, X. Y. Yue, G. Niu, M. Yang, D. X. Cui, X. Y. Chen, *Biomaterials*, 2013, **34**, 4643.
5. C. C. Bao, N. Beziere, P. del Pino, B. Pelaz, G. Estrada, F. R. Tian, V. Ntziachristos, J. M. de la Fuente, D. X. Cui, *Small*, 2013, **9**, 68
6. P. Huang, O. Pandoli, X. S. Wang, Z. Wang, Z. M. Li, C. L. Zhang, F. Chen, J. Lin, D. X. Cui, X. Y. Chen, *Nano Res.*, 2012, **5**, 630.
7. P. Huang, L. Bao, C. L. Zhang, J. Lin, T. Luo, D. P. Yang, M. He, Z. M. Li, G. Gao, B. Gao, S. Fu, D. X. Cui, *Biomaterials*, 2011, **32**, 9796.
8. A. Bianco,M. Prato, *Adv. Mater.,* 2003, **15**, 1765
9. D. Iannazzo, A. Piperno, A. Pistone, G. Grassi,S. Galvagno, *Curr. Med. Chem.*, 2013, **20**, 1333.
10. P. Huang, J. Lin, X. Wang, Z. Wang, C. Zhang, M. He, K. Wang, F. Chen, Z. Li, G. Shen, D. Cui, X. Chen, *Adv. Mater.*, 2012, **24**, 5104.
11. C. Liu, P. Zhang, X. Zhai, F. Tian, W. Li, J. Yang, Y. Liu, H. Wang, W. Wang,W. Liu, *Biomaterials,* 2012, **33**, 3604.
12. K. Yang, L. Feng, X. Shi, Z. Liu, *Chem. Soc. Rev.*, 2013, **42**, 530.
13. Z. Li, J. C. Barnes, A. Bosoy, J. F. Stoddart, J. I. Zink, *Chem. Soc. Rev.*, 2012, *41*, 2590.
14. N. Z. Knezevic,V. S. Y. Lin, *Nanoscale*, 2013, **5**, 1544.

15. X. Fang, X. Zhao, W. Fang, C. Chen,N. Zheng, *Nanoscale,* 2013, **5**, 2205.
16. W. Fan, B. Shen, W. Bu, F. Chen, K. Zhao, S. Zhang, L. Zhou, W. Peng, Q. Xiao, H. Xing, J. Liu, D. Ni, Q. He, J. Shi, *J. Am. Chem. Soc.*, 2013, **135**, 6494.
17. J. Liu, W. Bu, L. Pan, J. Shi, *Angew. Chem. Int. Ed.*, 2013, **52**, 4375.
18. P. Fratzl, H. S. Gupta, E. P. Paschalis, P. Roschger, *J. Mater. Chem.,* 2004, **14** , 2115.
19. M. Tzaphlidou, *J. Biol. Phys.,* 2008, **34**, 39.
20. C. E. Hoffler, X. E. Guo, P. K. Zysset, S. A. Goldstein, *J. Biomech. Eng.-T. Asme.,* 2005, **127**, 1046.
21. A. K. Bembey, A. J. Bushby, A. Boyde, V. L. Ferguson,M. L. Oyen, *J. Mater. Res.,* 2006, **21**, 1962.
22. J. L. Ong, D. C. N. Chan, *Crit. Rev. Biomed. Eng.,* 2000, **28**, 667a.
23. F. Chen, Y. J. Zhu, J. Wu, P. Huang, D. X. Cui, *Nano. Biomed. Eng,* 2012, **4**, 41.
24. F. Chen, C. Li, Y. J. Zhu, X. Y. Zhao, B. Q. Lu, J. Wu, *Biomater. Sci.*, 2013, **1**, 1074.
25. J. Zhao, Y.J. Zhu, J.Q. Zheng, F. Chen, J. Wu, *Micropor. Mesopor. Mater.*, 2013, **180**, 79.
26. J. H. Adair, E. I. Altinoglu, T. J. Russin, J. M. Kaiser, B. M. Barth, P. C. Eklund,M. Kester, *ACS Nano* 2008, **2**, 2075.
27. F. Chen, P. Huang, Y. J. Zhu, J. Wu, D. X. Cui, *Biomaterials,* 2012, **33**, 6447.
28. F. Chen, P. Huang, Y. J. Zhu, J. Wu, C. L. Zhang, D. X. Cui, *Biomaterials,* 2011, **32**, 9031.
29. M. Kester, Y. Heakal, T. Fox, A. Sharma, G. P. Robertson, T. T. Morgan, E. I. Altinoglu, A. Tabakovic, M. R. Parette, S. M. Rouse, V. Ruiz-Velasco, J. H. Adair, *Nano Lett.,* 2008, **8** , 4116.
30. T. T. Morgan, H. S. Muddana, E. I. Altinoglu, S. M. Rouse, A. Tabakovic, T. Tabouillot, T. J. Russin, S. S. Shanmugavelandy, P. J. Butler, P. C. Eklund, J. K. Yun, M. Kester, J. H. Adair, *Nano Lett,* 2008, **8**, 4108.
31. C. Qi, Y. J. Zhu, F. Chen, *Chem. Asian J.,* 2013, **8**, 88.
32. F. Chen, Y. J. Zhu, X. Y. Zhao, B. Q. Lu, J. Wu, *CrystEngComm*, 2013, **15**, 4527.
33. X. Y. Zhao, Y. J. Zhu, C. Qi, F. Chen, B. Q. Lu, J. Zhao, J. Wu, *Chem. Asian J.,* 2013, **8**, 1313.
34. G. F. Xu, I. A. Aksay, J. T. Groves, *J. Am. Chem. Soc.*, 2001, **123**, 2196.
35. Y. B. Li, D. X. Li, W. J. Weng, *J. Inorg. Mater.,* 2007, **22**, 775.
36. G. Balasundaram, M. Sato, T. J. Webster, *Biomaterials,* 2006, **27**, 2798.
37. K. S. W. Sing, D. H. Everett, R. A. W. Haul, L. Moscou, R. A. Pierotti, J. Rouquerol, T. Siemieniewska, *Pure Appl. Chem.,* 1985, **57**, 603.
38. S. M. Schmidt, J. McDonald, E. T. Pineda, A. M. Verwilst, Y. M. Chen, R. Josephs, A. E. Ostafin, *Micropor. Mesopor. Mater.,* 2006, **94**, 330.
39. J. Fan, J. Lei, C. Z. Yu, B. Tu, D. Y. Zhao, *Mater. Chem. Phys.,* 2007, **103**, 489.
40. Y. F. Zhao, J. Ma, *Micropor. Mesopor. Mater.,* 2005, **87**, 110.
41. S. X. Ng, J. Guo, J. Ma, S. C. J. Loo, *Acta Biomater.,* 2010, **6**, 3772.
42. D. L. Shi, *Adv. Funct. Mater.,* 2009, **19**, 3356.
43. K. Park, S. Lee, E. Kang, K. Kim, K. Choi, I. C. Kwon, *Adv. Funct. Mater.,* 2009, **19**, 1553.

Graphical Abstract

Mesoporous microspheres of Eu^{3+}-doped amorphous calcium phosphate are prepared using adenosine triphosphate by the microwave-assisted solvothermal method.